AGU PUBLICATIONS

Water Resources Research

RESEARCH ARTICLE
10.1002/2013WR014815

Special Section:
Patterns in Soil-Vegetation-Atmosphere Systems: Monitoring, Modelling and Data Assimilation

Seasonal soil moisture patterns: Controlling transit time distributions in a forested headwater catchment

Michael Paul Stockinger[1], Heye Reemt Bogena[1], Andreas Lücke[1], Bernd Diekkrüger[2], Markus Weiler[3], and Harry Vereecken[1]

[1]Forschungszentrum Jülich GmbH, Institute of Bio and Geosciences, Agrosphere Institute (IBG-3), Jülich, Germany, [2]Department of Geography, Bonn University, Bonn, Germany, [3]Chair of Hydrology, Albert-Ludwigs-Universität Freiburg, Freiburg, Germany

Key Points:
- Transit time distributions derived for river locations are heterogeneous
- Runoff-generating area reduces to riparian zone in the dry state
- Negative correlation between riparian zone area and mean transit time

Correspondence to:
M. P. Stockinger,
m.stockinger@fz-juelich.de

Citation:
Stockinger, M. P., H. R. Bogena, A. Lücke, B. Diekkrüger, M. Weiler, and H. Vereecken (2014), Seasonal soil moisture patterns: Controlling transit time distributions in a forested headwater catchment, *Water Resour. Res.*, *50*, doi:10.1002/2013WR014815.

Received 29 SEP 2013
Accepted 10 JUN 2014
Accepted article online 14 JUN 2014

Abstract The Transit Time Distribution (TTD) of a catchment is frequently used for understanding flow paths, storage characteristics, and runoff sources. Despite previous studies, the connections between catchment characteristics and TTDs are still not fully understood. We present results from a 2 year stable isotope tracer investigation in the forested Wüstebach headwater catchment (38.5 ha), including precipitation, stream, and tributary locations. We used the gauged outlet to determine effective precipitation (p_{eff}), subdivided for wet and dry catchment state, and assumed it to be spatially uniform. We then calculated TTDs of 14 ungauged stream and tributary locations where stable isotope tracer information was available and compared them to respective subcatchment areas and the proportion of riparian zone within the subcatchments. Our approach gave insight into the spatial heterogeneity of TTDs along the Wüstebach River. We found that hydrological hillslope-riparian zone disconnection was an important factor, as the catchment shifted between two distinct, time-variant hydrological responses that were governed by seasonal changes of overall catchment wetness. The difference in hydrological behavior of the riparian zone and hillslopes could explain the often encountered "old water phenomenon," where considerable amounts of old water quickly appear as runoff. TTD results showed a negative correlation between riparian zone proportion and Mean Transit Time (MTT), corroborated by the dense network of soil water content measurements. No correlation between subcatchment size and MTT was found.

1. Introduction

The distribution of transit times of precipitation (Transit Time Distribution (TTD)) and its average travel time (Mean Transit Time (MTT)) through a catchment to the outlet have been used in hydrological studies to investigate catchments in terms of, e.g., flow paths [*Pearce et al*., 1986] and storage [*Maloszewski et al*., 1992; *Soulsby et al*., 2009]. Since the TTD integrates different water transport mechanisms (e.g., overland flow, preferential flow, laminar subsurface flow, and ground water flow) that are controlled by catchment characteristics such as geology, land use, soil properties, and topography, dominant characteristics controlling runoff generation can theoretically be identified by comparison of respective TTDs. Such knowledge of the specific relation between the TTD and catchment characteristics becomes important when considering that catchment-wide water transport to the outlet has important implications for the catchment's sensitivity to anthropogenic influences, such as surface and groundwater pollution or land use change [*McGuire and McDonnell*, 2006]. However, the relation between catchment properties and TTDs is difficult to define because of catchment-specific heterogeneities and the lack of observational data with a high spatial and temporal resolution [*Tetzlaff et al*., 2008]. Furthermore, no method exists to directly measure catchment-wide water transport, making it difficult to verify or falsify results gained from inversely modeled TTDs.

Often the stable isotopes of water (δ^2H and δ^{18}O) are used as tracers in precipitation and runoff to derive TTDs. Usually, a highly variable precipitation tracer signal is time-shifted and attenuated by a transformation function (the TTD) to a less-variable runoff tracer signal.

In recent years, many studies have investigated the relationship between TTDs and catchment characteristics via different modeling approaches in several geographic and climatological settings. For instance, *Herrmann et al*. [1999] found that low permeability of bedrock and assumed average flow path lengths influence MTTs, with smaller subcatchments showing shorter transit times in a deep-soiled, wet

mountainous catchment. For catchments with well-drained, shallow soils, *McGuire et al*. [2005] found no direct relationship between catchment size and MTT and indicated that rather flow path characteristics than catchment size have a significant influence on TTDs. They found a decrease of transit times with increasing flow path gradient and an increase in transit times with increasing flow path length. In similar conditions, *Asano and Uchida* [2012] were able to link spatial differences in base flow MTTs to the depth of the hydrologically active soil (d_m) and bedrock for mountainous catchments with shallow soils. They argue that contrasting relationships of topographic indices and MTT found in previous studies [e.g., *McGuire et al*., 2005; *Rodgers et al*., 2005; *Tetzlaff et al*., 2009b] could be a result of d_m being not always linked to topography. Even at sites where topography and d_m are related to each other, they argue that the relationship should vary across different sites.

The relationship between the ratio of riparian to hillslope zone surface area and water and solute transport have been investigated by *McGlynn and Seibert* [2003] in headwater catchments. They argue that headwater catchments are influenced by riparian zones, because they can efficiently buffer hillslope-generated runoff. However, the capacity of the riparian zone to buffer water and solute transport may become negligible in the case of large catchments. To compare different geographical regions and their effects on the control of topography on TTDs, *Tetzlaff et al*. [2009b] investigated 55 catchments in different geographical settings by comparing topographic indices such as distance from stream or average gradient derived from a Digital Elevation Model (DEM) to a proxy of TTD (ratio of standard deviation of a tracer signal in stream water to the standard deviation of the tracer signal in precipitation). They found that the controls of the investigated topographic indices on TTDs vary among different geomorphological regions, including glaciated steep mountainous and hilly, forested catchments. These studies demonstrate that transferring knowledge from one catchment to another catchment as well as hydrological catchment classification are complex tasks that sometimes require detailed knowledge of a catchment's characteristics. Further complications in finding controlling factors for TTDs may arise due to the assumptions of linearity and stationarity of TTDs [*Rinaldo et al*., 2011] and uncertainties in input data and models.

Identifying links between TTDs and changes in catchment characteristics is even more challenging, e.g., in the case of catchments which are strongly influenced by groundwater and, as a consequence, usually are characterized by longer transit times [e.g., *Stewart and Fahey*, 2010]. They showed that shallow aquifers and deep aquifers within the bedrock were controlling the TTDs, while the afforestation of the modeled catchment in the 1980s had not yet affected deep storage flow in 2009.

The difficulties and ambiguities in identifying the relative effect of catchment characteristic on TTDs of catchments of a wide variety of geographical and climatological conditions were summarized by *Hrachowitz et al*. [2009a]. They used long-term data sets in 20 different headwater catchments, ranging from <1 to 35 km^2 in size and found that no single dominant catchment characteristic controlled TTDs. Rather, an ensemble of soil cover, precipitation patterns, stream structure, and topography worked well in estimating TTDs in a multiple regression model.

This and previous studies focused either on topography-derived measures or spatiotemporally limited measurements to explain possible mechanisms that had influenced obtained TTD results. What is currently lacking in hydrology are studies that allow hypothesis about the relation of catchment characteristics and TTDs based on high-resolution spatiotemporal measurements, constraining possible solutions to the question why these results have been obtained [*McDonnell et al*., 2010].

In this study, we used data from a high-resolution spatiotemporal measurement network to investigate the spatial pattern of TTDs of ungauged subcatchments of the mountainous, forested Wüstebach headwater catchment (38.5 ha), and one tributary catchment (11 ha). We then compared the TTDs to subcatchment characteristics (size and riparian zone area). Therefore, the objectives of this study were to derive an approach to determine subcatchment TTDs of ungauged stream locations, to investigate spatial variability of TTDs within the catchment, and to use the available dense soil moisture measurement network to explain spatial patterns of TTDs.

2. Study Site

2.1. The Wüstebach Headwater Catchment

The Wüstebach headwater catchment (38.5 ha) is located in the humid temperate climatic zone with a mean annual precipitation of 1107 mm (1961–1990) and a mean annual temperature of 7°C [*Zacharias*

et al., 2011]. Note that in *Bogena et al*. [2010] and subsequent publications [e.g., *Rosenbaum et al*., 2012], the catchment size is given as 27 ha. This difference is the result of using a new DEM in this study, with a resolution of 1 m (before: 10 m). Based on this new DEM, we added an area south of a federal road as part of the catchment, increasing its size to 38.5 ha [see also *Graf et al*., 2014].

The catchment is located in the low mountain reaches of Western Germany (50°30′16″N, 6°20′00″E, WGS84) at about 595–628 m above sea level (asl.). The Wüstebach site is part of the Lower Rhine/Eifel Observatory of the Terrestrial Environmental Observatories (TERENO) network [*Zacharias et al*., 2011]. It belongs to the Eifel national park and is dominantly covered by Norway spruce (*Picea abies*) and Sitka spruce (*Picea sitchensis*) [*Etmann*, 2009]. The bedrock consists of Devonian shales with sporadic inclusions of sandstone [*Richter*, 2008]. It is covered by two periglacial layers: a "top layer" with a mean depth of about 50 cm throughout most of the catchment [*Borchardt*, 2012] and a "base layer" of varying depths (50–150 cm). The base layer has a higher bulk density and thus lower hydraulic conductivity than the top layer [*Borchardt*, 2012]. Soil depths in these periglacial layers range from less than 1 m to a maximum of 2 m with an average depth of 1.6 m [*Graf et al*., 2014]. Food and Agriculture Organization (FAO) soil types of cambisol and planosol/cambisol are dominantly found on the hillslopes while gleysols, histosols, and planosols are found in the riparian zone.

We additionally investigated a smaller tributary-catchment (11 ha, not included in the 38.5 ha) situated north-east of the Wüstebach test site, which is also part of the weekly sampling campaign described in section 2.2. This subcatchment drains into the Wüstebach a few meters downstream of the catchment's outlet (Figure 1).

2.2. Measured Data

For this study hydrological and isotopic measurements from 6 June 2009 to 31 March 2011 were used. Discharge was measured at the catchment's outlet equipped with a V notch weir for low-flow measurements and a Parshall flume to measure medium to high flows. The precipitation time series with a temporal resolution of 1 h and a 0.1 mm measurement increment was acquired from the meteorological station Kalterherberg (German Weather Service, station number 80115, 535 m asl.) located approximately 5 km west of the Wüstebach catchment. Daily snow height data with 1 cm resolution from Kalterherberg station was used with a simple snow model to account for snow storage retardation effects (see section 3.2).

The acquisition of weekly stream and tributary water grab samples for analysis of stable isotopes of water started on 18 May 2009. We sampled 50 mL of stream water from each of the 15 different locations along the Wüstebach main stream and its tributaries (see Figure 1). Due to infrequent water flow, sampling location 7 was not included in this study. Weekly precipitation samples for isotopic analysis were collected since 8 June 2009 from a wet deposition collector at the close-by TERENO meteorological station Schöneseiffen (620 m asl., approximately 3.5 km to the NE), as there is no rainfall sampler at Kalterherberg station. The precipitation water was collected by a funnel (200 cm^2) connected to a 2.3 L high-density polyethylene (HDPE) bottle via plastic tubing. The samples were cooled in situ to 4°C in a standard refrigerator. As the collection funnel was not heated, it is unknown if all snowfall eventually melted into the collection funnel or if losses occurred due to snow cover buildup. In the beginning of 2010, we were not able to gather precipitation isotope samples for almost 3 months, leading to a very coarse bulk sample during this time. Nevertheless, we used this 3 month bulk sample, as during this 3 month sampling gap evaporation was limited (winter with low-ambient air temperatures) and the accumulated precipitation amounts did not exceed the maximum storage capacity of the collection bottle.

The isotopic analysis of water samples was carried out using Isotope-Ratio Mass Spectrometry (IRMS) with high-temperature pyrolysis to analyze $\delta^{18}O$ and $\delta^{2}H$. Isotope values are given as δ values and are reported on the Vienna Standard Mean Ocean Water (VSMOW) scale [*Gonfiantini*, 1978]. Several in-house laboratory standards calibrated against VSMOW, Standard Light Antarctic Precipitation (SLAP2), and Greenland Ice Sheet Precipitation (GISP) were used to calibrate the measurements and to guarantee long-term stability of our analyses during the investigation period. The analytical accuracy of our IRMS is $\leq 0.1‰$ for $\delta^{18}O$ and $\leq 1.0‰$ for $\delta^{2}H$.

Hourly soil water content data at three depths (5, 20, and 50 cm) used in this study stem from the wireless sensor network SoilNet installed in the Wüstebach test site (Figure 1) [*Bogena et al*., 2010].

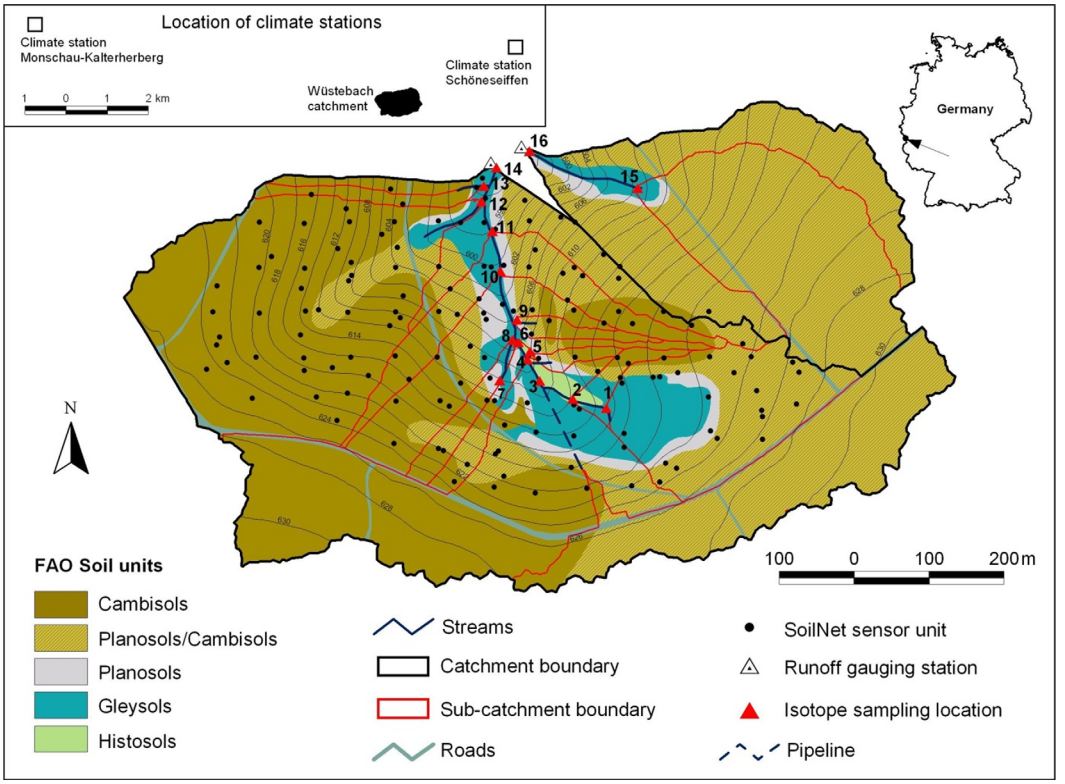

Figure 1. Map of the 38.5 ha Wüstebach headwater catchment (outlet: location 14), with the smaller 11 ha tributary catchment (outlet: location 16) adjacent to the north-east. Displayed are FAO soil units, isolines and stream/tributary locations for water sampling (numerals). Due to constantly low-water levels, we were not able to use location 7 for this study. Runoff gauging stations are marked with open triangles. Black dots mark SoilNet sensor units for soil moisture measurements. Subcatchments of each measurement location are given as red outlines. Note that subcatchment 3 receives water from a pipe, originating from an artifical water catchment system south of location 3. The inset shows the location of the meteorological stations used.

3. Methods

3.1. Data Preparation

We combined runoff data of the two gauges by using V notch values for water levels below 5 cm (equal to 2.9 m^3/h), Parshall flume values for water levels greater than 10 cm (equal to 56.9 m^3/h), and a weighted mean value in between those water levels (all water levels refer to measurements at the V notch weir). V notch discharge was calculated from the Thomson weir equation and Parshall flume discharge (uncertainty of about 3%) from a rating curve provided by its manufacturer. We then averaged the discharge measurements to hourly resolution.

The precipitation time series from the Kalterherberg station was checked for consistency by comparison to the Schöneseiffen station. One large rainfall event (3 July 2009, 12:00 PM) with an intensity of 27.7 mm/h did not show any corresponding reaction in the hydrograph or in soil water content. We therefore assumed that a convective storm cell had passed over the Kalterherberg station but did not cross the Wüstebach catchment. Consequently, we substituted this measurement with data from the Schöneseiffen station that recorded only 1.8 mm/h. The measured Kalterherberg precipitation data series was corrected for losses due to evaporation and wind drift according to *Richter* [1995]. The correction resulted in an overall increase of the total rainfall during the modeling period by 13% (from 2209.7 to 2508.4 mm), and in an improved closure of the catchment's water balance [*Cornelissen et al*., 2014; *Graf et al*., 2014].

We selected 111 SoilNet locations from the total number of 150 sensor nodes in order to have a continuous time series. The three depths (5, 20, and 50 cm) were summed up to calculate the weighted mean soil water content (*SWCm*) for a 1.6 m soil column. The 5 and 20 cm SWC measurements were given weights of 0.1 and 0.2, representing the depths of 0–0.1 and 0.1–0.3 m respectively, with the 50 cm measurement receiving a weight of 1.3, representing the remaining depth of 0.3–1.6 m.

3.2. Snow Melt Model

We used a simple snow melt model to account for the delay of precipitation input due to storage as snow. During times of snow cover buildup, precipitation is accumulated in a snow storage component. In the case of partial melt of the snow cover, defined as decrease in measured snow cover height and expressed in percent, a corresponding percent of melt water is uniformly released over an arbitrarily chosen time period of 6 h. A sensitivity analysis with snow melt periods between 3 and 6 h showed negligible impact on the results. We are aware of the fact that compaction of the snow cover can account for decreasing snow cover height. In this study, we assumed that compaction accounts for markedly smaller changes than partial melt, keeping possible errors due to this simplification to a minimum. In the case of complete melt of the entire snow cover, all stored water was uniformly released over a time period of 6 h. We acknowledge the simplicity of the snow model and that 6 h might be too short for complete snow cover meltdown in some cases. However, the use of our snow melt model in rainfall-runoff simulations showed no major hydrograph simulation misfits owing to this approach, as the eventual release of snow cover stored rainfall inputs coincided well with observed runoff events. As snow accumulation and melting happens only a few times during the 2 year modeling period, we assume that a more advanced snow model would not lead to a significant increase in the runoff simulation performance.

3.3. Determination of the Transit Time Distributions

For hydrograph simulation we used the conceptual rainfall-runoff transfer function hydrograph separation model (TRANSEP) [*Weiler et al*., 2003], which inversely solves equations (1) and (2) on the basis of observed runoff time series, to calibrate the effective precipitation time series p_{eff}. Determination of p_{eff} is based on a nonlinear Antecedent Precipitation Index (API) approach [*Jakeman and Hornberger*, 1993]

$$p_{eff}=p(t)s(t) \tag{1a}$$

$$s(t)=b_1p(t)+\left(1-b_2^{-1}\right)s(t-\Delta t) \tag{1b}$$

with $p(t)$ the measured precipitation, $s(t)$ the API, Δt the calculation time step of 1 h, b_1 a scaling factor to match the amount of total simulated runoff to the amount of total effective precipitation and b_2 weighing each precipitation event backward in time. An additional parameter, b_3, sets the initial API conditions for time step $t = 0$.

The hydrograph is calculated using

$$Q(t)=\int_0^t g(\tau)p_{eff}(t-\tau)d\tau \tag{2}$$

with $Q(t)$ being the calculated runoff, $g(\tau)$ the Response Time Distribution (RTD), τ is the response time, and $p_{eff}(t-\tau)$ the effective precipitation for time step $t-\tau$. The RTD is the hydrological response of the catchment to a unit rainfall input (similar to the unit hydrograph). While the RTD incorporates travel times of water molecules and celerities of hydraulic pressure waves propagating through the soil, the TTD only captures travel times of water molecules. As hydraulic pressure wave celerities can exceed travel times of water molecules by far, response times of a catchment are typically shorter compared to actual particle travel times [*Rinaldo et al*., 2011; *Roa-Garcia and Weiler*, 2010; *Williams et al*., 2002]. In TRANSEP several model types for the RTD and TTD are available: exponential model (E), exponential piston flow model (EP), dispersion model (D), gamma distribution (G), two parallel linear reservoirs (TPLR). Previous studies showed that the TPLR model produced good results in modeling TTDs [*Hrachowitz et al*., 2009b; *Weiler et al*., 2003]. In this study, we used two three-parameter TPLR models, each consisting of a fast and a slow responding reservoir, for both RTD ($g(\tau)$) and TTD ($h(\tau)$) simulation

$$g(\tau)=h(\tau)=\frac{\phi}{\tau_f}\exp\left(-\frac{\tau}{\tau_f}\right)+\frac{1-\phi}{\tau_s}\exp\left(-\frac{\tau}{\tau_s}\right) \tag{3}$$

with ϕ a fractionation factor between 0 and 1, partitioning a certain fraction of a unit precipitation input into the fast reservoir, τ_f and τ_s being the mean residence times of the fast and the slow reservoir,

respectively. Mean Response Times (MRTs) and Mean Transit Times (MTTs) are calculated as the 50% quantile of the respective cumulative RTD and TTD.

The parameters of the TPLR model (ϕ, τ_f, τ_s) and for the API calculation (b_1, b_2, b_3) were simultaneously optimized by the Ant Colony Optimization algorithm (ACO) [*Abbaspour et al*., 2001]. The ACO algorithm efficiently found the optimum solution in previous studies that also used TRANSEP [*Roa-Garcia and Weiler*, 2010; *Weiler et al*., 2003]. We chose the Volumetric Efficiency (VE) as the objective function [*Criss and Winston*, 2008]

$$VE = 1 - \frac{\sum |Q_{sim} - Q_{obs}|}{\sum Q_{obs}} \tag{4}$$

with Q_{sim} calculated and Q_{obs} observed runoff. Contrary to the commonly used Nash-Sutcliffe Efficiency (NSE) [*Nash and Sutcliffe*, 1970], the VE has the advantage that it equally weighs the residuals between observed and modeled runoff and does not put an emphasis on peak runoff. Since for this study weekly isotope samples taken mostly during low to moderate runoff conditions were available, VE is more appropriate for our runoff data.

The TTDs of gauged and ungauged stream and tributary isotope measurement locations can be modeled by using p_{eff}. Due to the small size of the Wüstebach catchment and its homogeneous land cover, we assumed the p_{eff} time series to be spatially representative for the whole catchment

$$C(t) = \frac{\int_0^t C_{in}(t-\tau) p_{eff}(t-\tau) h(\tau) d\tau}{\int_0^t p_{eff}(t-\tau) h(\tau) d\tau} \tag{5}$$

with $C(t)$ stream water isotope values at time t, $C_{in}(t-\tau)$ precipitation isotope values at time t with travel time τ and $h(\tau)$ the TTD. We used δ^{18}O and δ^{2}H to model several locations; as the results were similar, we solely used δ^{18}O data for modeling of all sampling locations. As we used a spin-up period of 2 years in isotope modeling, initial TTD results had to be rescaled to the modeling time frame of 665 days by leaving out the 2 years of spin-up. To do this, we summed the initial results corresponding to the time frame of 0–665 days transit time and divided each by the sum of these values, so that their final cumulative sum equaled unity. This implicitly assumes that 100% of the tracer leaves the catchment within 665 days. As the conductivity of the shale bedrock at the Wüstebach catchment is extremely low (10^{-7} to 10^{-9} m/s) [*Graf et al*., 2014], we assumed that the contribution of deep groundwater to total runoff with transit times longer than 665 days is negligible. Furthermore, we assumed that the contribution from the shallow soil water reservoir and the riparian zone in the Wüstebach catchment has a turnover time shorter than 665 days.

To optimize the TTD simulation, we used the ACO algorithm and the NSE measure, as we modeled the complete isotope tracer time series with an emphasis on dynamics in the time series (i.e., isotope peaks in the time series). The NSE is given as

$$NSE = 1 - \frac{\sum (C_{obs} - C_{sim})^2}{\sum (C_{obs} - \overline{C_{obs}})^2} \tag{6}$$

with C_{sim} the simulated isotope concentration in the stream, C_{obs} the observed isotopic concentration in the stream, and $\overline{C_{obs}}$ the mean value of all observations. Additionally, we computed the VE for the optimized isotope results (with absolute values in the denominator of equation (4) to account for negative δ^{18}O) to compare NSE and VE values for each location.

For analysis of correlations between catchment characteristics and spatial TTDs patterns, we derived the subcatchment areas of all stream isotope sampling locations using the single flow direction algorithm as described in *Jenson and Dominique* [1988] of the software ArcView (ESRI, Redlands, CA).

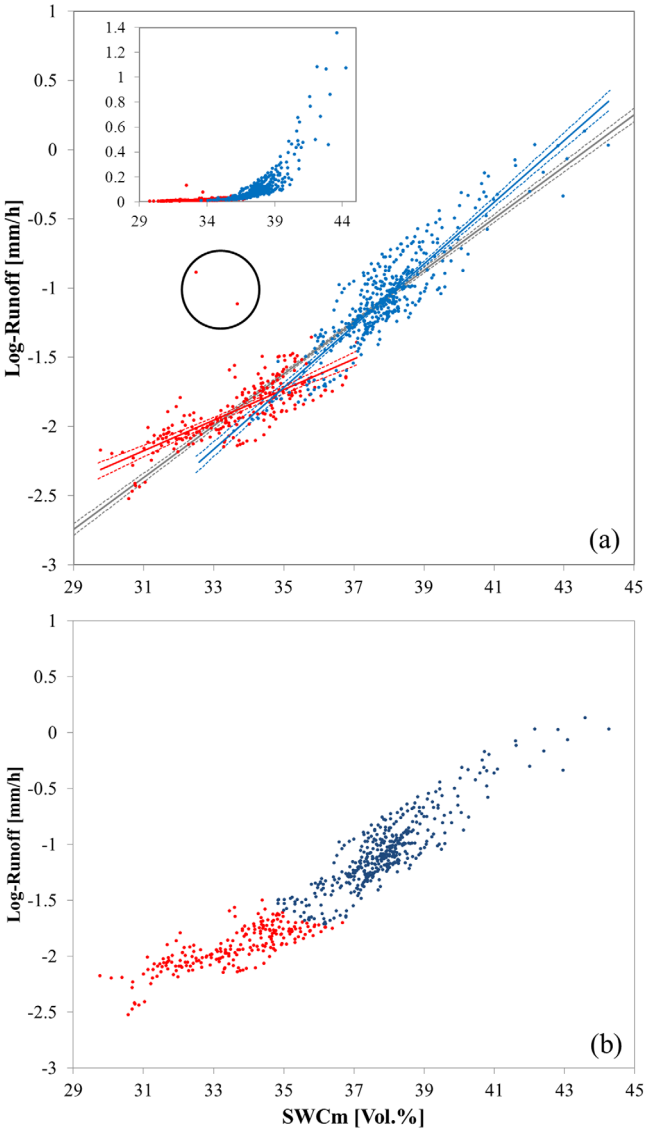

Figure 2. (a) Daily mean runoff (log-transformed, base: 10) against *SWCm* for dry states (red dots) and wet states (blue dots), respectively (dates in Table 1). Inset shows runoff against *SWCm*. Correlation and 95% confidence interval for dry states (red solid and dashed lines) with Log-Runoff = 0.110 *SWCm* − 5.597 with $R^2 = 0.53$, wet states (blue solid and dashed lines) with Log-Runoff = 0.223 *SWCm* − 9.525 with $R^2 = 0.81$ and both combined (gray solid and dashed lines) with Log-Runoff = 0.187 *SWCm* − 8.173 with $R^2 = 0.88$, all three with significance value $p < 10^{-39}$. Outlier values are marked with a black circle. (b) Result of cluster analysis without outliers using the initial assumption of two clusters (red and blue dots).

3.4. Splitting the Hydrograph Into Submodeling Periods

At an early stage of hydrograph simulation, we simulated the entire study period and found that the model overestimated runoff in summer and underestimated it in winter (not shown). It was not possible to capture the annual variability of the catchment's hydrological behavior using a single optimized parameter set. Thus, we had to derive a method to split the hydrograph into distinct submodeling periods where the catchment's hydrological behavior would be quasi-constant, allowing for hydrograph simulation with one single parameter set for each period.

In accordance with *Graf et al.* [2014], we found that at a *SWCm* value of about 35 vol % the relation between daily mean runoff and soil water storage changes. In winter, when *SWCm* is generally higher than 35 vol %, we found a higher slope between *SWCm* and runoff than during summer, when *SWCm* is generally lower than 35 vol % (Figure 2a). Based on this, we divided the 2 year time series into four submodeling time series, splitting the hydrograph at points where *SWCm* values of 35 vol % were exceeded for a longer period of time. We did not split the hydrograph at (a) short-term exceedances of a few days and (b) an approximately 10 day exceedance in mid-May 2010, where before and after values dominantly stayed below 35 vol %. The divisions of the complete hydrograph time series fall almost exactly on hydrological half-year dates with 1 November 2009, 1 May 2010, and the exception of 15 August 2010. Accordingly, the four periods are indicated as: "Summer_09," "Winter_09," "Summer_10," and "Winter_10," respectively, and the Wüstebach's dry (*SWCm* < 35 vol %) and wet state (*SWCm* > 35 vol %) are simply referred to in the following as "dry state" and "wet state."

To test the validity of the subjectively chosen *SWCm* value for splitting the hydrograph, we used an expectation-maximization (EM) algorithm to objectively find data clusters in the relationship between runoff and *SWCm* [*Fraley and Raftery*, 2002]. We tested 1–4 clusters and compared their maximum likelihood value, leaving out two outlier runoff events during summer months. The likelihood for two clusters was higher

than for one cluster, with the algorithm splitting the data points in a range from 35 to 37 vol % (Figure 2b). Higher-order cluster analysis (i.e., using three or four clusters) were rejected because they resulted in a similar cluster split compared to the two cluster analysis.

The p_{eff} of the high-intensity (31 mm/h) event of 3 July 2010 was estimated separately as it met dry topsoil conditions and resulted in preferential subsurface flow, leading to a rapid runoff response [see *Rosenbaum et al*., 2012]. This would result in a unique RTD compared to the rest of this summer's modeling period. To derive the p_{eff} of this event, we used the sum of the first 2 h of the event runoff as they showed a fast and markedly increase compared to the situation prior and subsequent these 2 h. We then subtracted the mean runoff of the 3 days prior to this event (low-flow conditions and thus, we assumed, base flow) to calculate the event fraction of the runoff reaction. We assumed this event fraction to be p_{eff} for the 3 July 2010 storm event.

For further analysis of the individual modeling periods, we additionally calculated the runoff coefficient *C* as the ratio of precipitation to runoff amounts for each period.

3.5. Adaption of Stable Isotopes in Precipitation

Catchment-scale lumped parameter models utilizing tracers are based on the assumption that representative model inputs are used [*McGuire and McDonnell*, 2006]. Our study catchment is forested while we used precipitation isotope data from open land. Precipitation passing through canopy generally increases in isotope values compared to open land precipitation [*Allen et al*., 2013; *Saxena*, 1986]. Due to the uncertainties of the canopy-influence on rainfall isotope values, we used the simple approach of adding an overall mean change to all isotope rain values.

We acknowledge the simplicity of this approach and the unknown uncertainties it introduced into the TTD modeling process and are currently conducting an experiment designed to further investigate this issue.

4. Results

Overall, there were no long-term hydrological extremes in precipitation or runoff (Figure 3), with neither of the investigated years being too dry or too wet compared to the long-term precipitation mean (1107 mm, without approximately 13% increase due to correction for evaporation and wind drift [*Richter*, 1995]). This is reflected in total precipitation and runoff, which amounted to 2508.4 and 1266.9 mm, respectively, indicating 49% evapotranspiration (ET) losses and storage change. Only one extreme storm event occurred, leading to a pronounced recharge response in *SWCm* (refer to Figures 3a and 3b, "Summer_10"). During both winters, base flow water levels rose to the approximately same level, with multiple event hydrographs sharing similarities in behavior. The *SWCm* reacted very similar to the hydrograph (Figure 3b). Isotopically, the modeling period also did not show any unexpected extremes. δ^{18}O in precipitation had a typical seasonal variation with enriched isotope values during summer and depleted values during winter months. In comparison, stream isotope values were heavily attenuated compared to the amplitudes observed in precipitation (Figure 3c). Stream isotope observations ranged from approximately -9.0 to -7.0 δ^{18}O, with precipitation samples ranging from approximately -14.0 to -2.5 δ^{18}O. Plotting isotope values of precipitation in the delta space plot (δ^{18}O versus δ^{2}H), we determined the Local Meteoric Water Line (LMWL). We found that the stream isotope values were slightly shifted from the LMWL (Figure 4). However, the average of all stream isotope values ($\delta^{18}\mathrm{O} = -8.37$, $\delta^{2}\mathrm{H} = -52.23$) almost matched with the LMWL.

4.1. Hydrograph Simulation

Hydrograph simulation results are shown in Figure 3a, while Table 1 lists the six optimized parameters, the VE, the runoff coefficient *C* and the MRT for each period. The model was able to fit all periods equally well, with VE values of 0.76, 0.55, 0.65, and 0.64, respectively. We found p_{eff} for the 3 July 2010 event to be 19.8 mm/h, meaning that 64% of gross precipitation appeared as immediate event runoff.

Cumulative RTDs for the dry and the wet state are shown in Figure 5. We initially calculated parameter sets for each modeling period separately. As the two dry states showed negligible differences in parameters, with the same being true for both wet states, we assumed that the catchment's hydrological reaction in both dry and wet states did not change significantly during the modeling period. Therefore, based on model performance we decided to use one parameter set (Summer_09) for both dry states and one

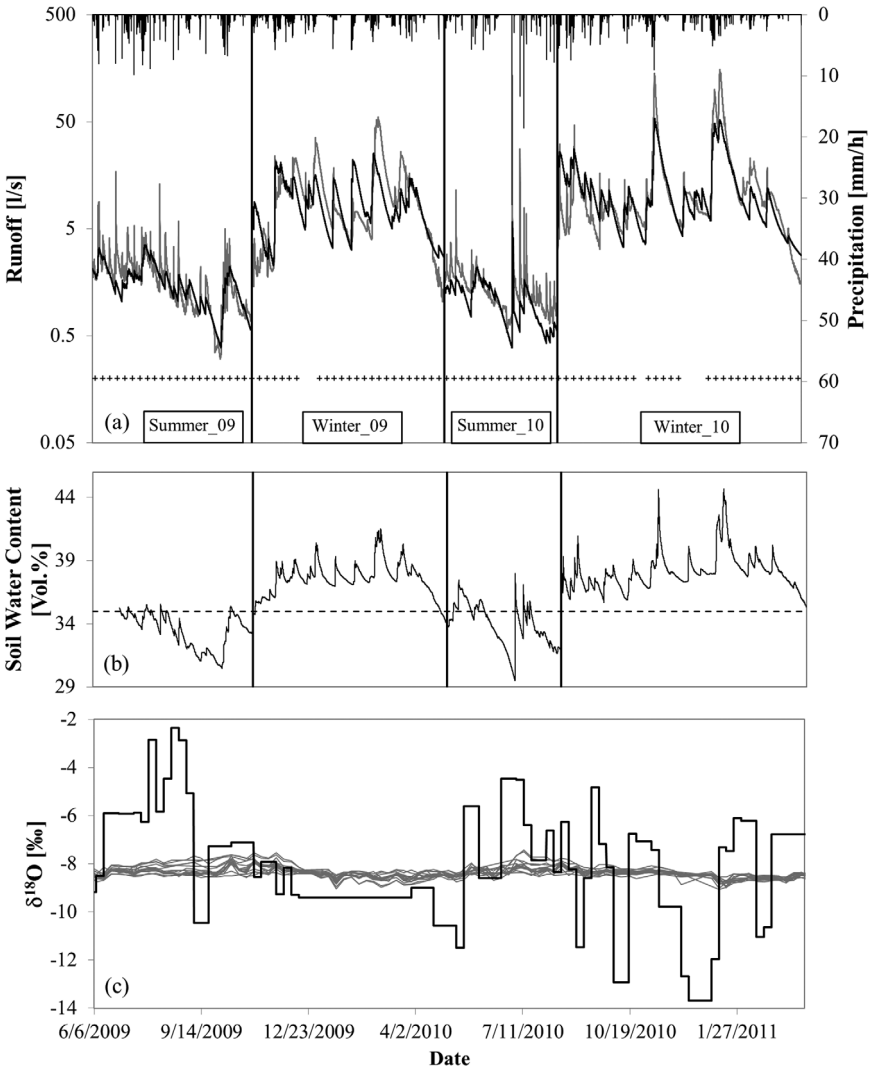

Figure 3. Time series (6 June 2009–31 March 2011) of (a) observed (gray line) and simulated runoff (black line) in logarithmic scale, precipitation (black bars from top), stream water sampling times (black crosses) for two summer and two winter seasons, (b) depth-weighted average soil water content *SWCm* and threshold of 35 vol % (dashed line), and (c) isotope data for all stream water locations (gray lines) and precipitation (black line). Black vertical lines in Figures 3a and 3b are hydrograph modeling periods based on *SWCm*. As isotope modeling has not been split up, no modeling periods are shown in Figure 3c.

(Winter_10) for both wet states. The RTD of the dry state first shows a slower reaction than that of the wet state, but then reacts much faster beginning at 13 days response time. Although hydrograph modeling during dry state is focusing on low to medium flows only, the dry state periods lacked a slow component in comparison to the wet states, with 99.5% of response times within 66 days during dry state and 205 days during wet state, respectively. Contrary to this, the wet state periods have both a fast and a slow component. This indicates that water following slower flow paths does not reach the outlet during dry state. Due to these RTD results, we had to recalculate p_{eff} for the dry state periods. In doing so, we postulate that the obtained RTDs indicate that during the wet state the whole Wüstebach catchment is hydrologically active, while during the dry state only the riparian zone contributes to runoff. The reduction in runoff contributing area increases the precipitation-equivalent runoff, which directly affects dry state p_{eff} and thus stream isotope simulations and their respective TTDs (see equation (5)).

In the course of recalculating p_{eff} for dry state, we tested if the increased runoff amounts (in mm) would not exceed total precipitation amounts (in mm). We, therefore, used the already obtained RTD to simulate runoff for both dry states separately with varying contributing areas ranging from 1 ha (corresponding to runoff amount increase of 3700%) to 8 ha (increase of 375%). We found that from 1 to 4 ha there was not

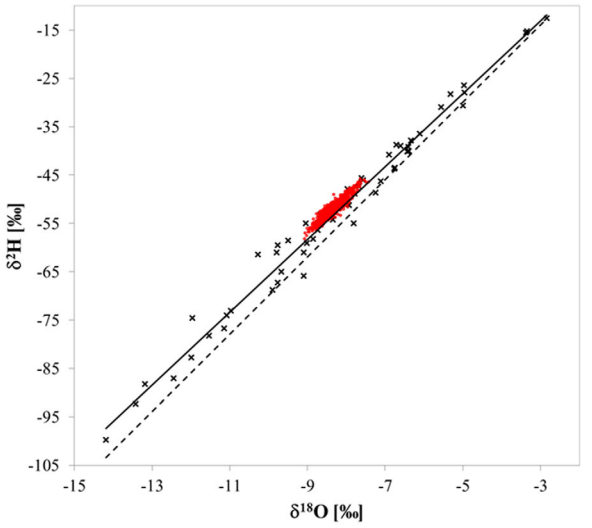

Figure 4. Isotopic composition of precipitation (crosses) and Local Meteoric Water Line (LMWL) for the observation period (solid line) compared with the Global Meteoric Water Line [*Craig*, 1961] (GMWL, dashed line). LMWL has an R^2 of 0.98 with $\delta^2H = 7.549\ \delta^{18}O + 9.611$. Stream isotopes samples of all 15 stream locations are slightly shifted from the LMWL (red dots).

enough rain to match runoff amounts, which led to very poor model performances. Starting with 5 ha, precipitation amounts sufficed and the Root Mean Square Error (RMSE) reached a low plateau (Figure 6 and also see runoff coefficients of Table 1). This value corresponds well with the extent of the riparian zone in the soil map (Figure 1). Using 5 ha catchment-area for dry state conditions resulted in an increase of precipitation-equivalent runoff by 770% compared to the 38.5 ha catchment. Corresponding runoff coefficients *C* are 1.08 and 0.98 for both dry states (5 ha) and 1.67 and 1.34 during wet state (38.5 ha) periods (Table 1). The low *C* in each dry state is attributable to only the riparian zone generating runoff, in which nearly all of precipitation creates a runoff response.

Thus, the final p_{eff} time series is a composite of four modeling periods with alternating runoff contributing areas. Total p_{eff} was 1607 mm, which is 64% of the total precipitation. The remaining 36% of total precipitation are either lost to ET and storage changes or appear as runoff in the not simulated hydrograph parts (e.g., rainfall-runoff events during dry state).

4.2. Stream Isotope Modeling

We found the overall mean change in isotope values from open land precipitation to throughfall to be 0.5‰ in $\delta^{18}O$ after calibration. The simulation performance increased by 0.11 in NSE, exemplary for a stream location near the spring of Wüstebach (location 1, see Figure 1). In general, the precipitation isotope time series showed a higher variability than the stream isotope time series, as transport through the catchment delays and attenuates the precipitation isotope signal. However, only a few stream locations showed similar, but attenuated, seasonal variations, with some locations showing almost none at all (e.g., location 3, 12, 15).

To further test the hypothesis of a partial contributing area of 5 ha during dry state, we simulated stream $\delta^{18}O$ values at measurement locations 1 and 14 with two approaches. First, we assumed a constant active catchment area of 38.5 ha in the derivation of p_{eff}, and second we used a season-dependent active catchment area approach with 38.5 ha during wet state and 5 ha during dry state. The comparison of both

Table 1. Optimized Parameters of the Rainfall-Runoff Model for the Four Modeling Seasons[a]

	Summer_09	Winter_09	Summer_10	Winter_10
	6/6/2009–10/31/2009	11/1/2009–4/30/2010	5/1/2010–8/15/2010	8/15/2010–3/31/2011
C	1.08	1.67	0.98	1.34
b_1	0.39	0.08	0.50	0.11
b_2	1.37	10.00	10.00	7.00
b_3	0.83	0.00	0.65	0.00
τ_f (d)	4	7	4	7
τ_s (d)	13	72	13	72
ϕ (−)	0.00	0.70	0.00	0.70
MRT (d)	9	7	9	7
VE	0.76	0.55	0.65	0.64

[a]C, runoff coefficient; b_1, scaling parameter; b_2, precipitation weighing parameter; b_3, API at t = 0; τ_f, fast reservoir mean residence time in days for RTD g(τ); τ_s, slow reservoir mean residence time in days for RTD g(τ); ϕ, fast reservoir contribution for RTD g(τ); MRT, mean response time; VE, volumetric efficiency.

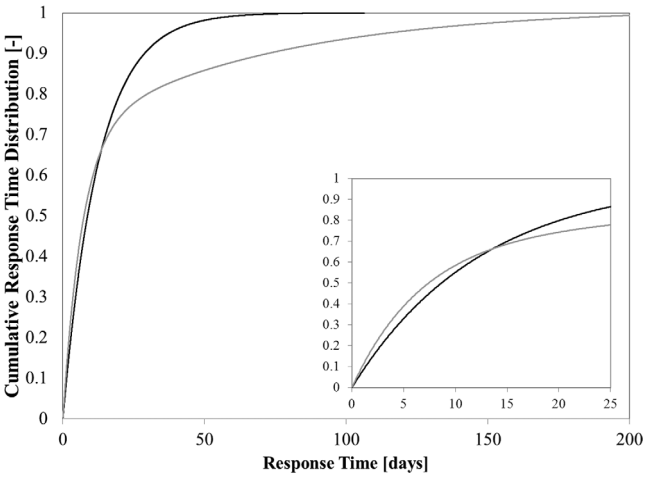

Figure 5. Cumulative RTDs for the dry (black line) and the wet state (gray line) for the outlet of the Wüstebach catchment (location 14). Inset shows details from 0 to 25 days response time.

approaches (see Figure 7) showed that a catchment area of 38.5 ha for the whole period resulted in poorer simulation result (NSE = 0.45) than using 38.5 ha during wet and 5 ha during dry state periods (NSE = 0.74) for location 1. In the case of location 14, the model performance slightly decreased from the 38.5 ha only (NSE = 0.37) to the 38.5 and 5 ha simulation (NSE = 0.34).

Isotope simulation results are shown exemplary for locations 1 and 14 in Figure 7, while all TTD results are summarized in Figure 8a. Table 2 lists the objective function values, parameters, and subcatchment characteristics for each location, respectively. Comparison of all TTDs in Figure 8a revealed that the outlet (location 14) is indeed an integration of the catchment's spatially different response to precipitation input, integrating shorter and longer transit times [*Shaman et al.*, 2004]. The NSE for all 15 stream locations ranged between −0.09 and 0.74, with VE values ranging between 0.9788 and 0.9897. Note that the small variability of the VE values is due to the reformulation of equation (4) with $\delta^{18}O$ values instead of runoff, leading to more subtle differences. We found that locations that have a high NSE usually have a low VE and show more dynamics in their isotope time series (not shown) with shorter MTTs compared to locations with a low NSE and high VE that have less dynamic isotope time series and longer MTTs (Figure 8b and Table 2). The outlet (location 14) integrated different NSE and VE values comparable to its integration of the different TTDs.

From location 1 (near the spring) downstream to the outlet (location 14) we generally found increasing MTTs for main stream locations (Figure 8a and Table 2; see Figure 1 for locations). Exceptions to this rule were locations 10 and 11, in which location 10 showed a shorter MTT than the upstream location 6, and 11 showed a longer MTT than the downstream outlet 14. Comparison of the TTDs of locations 10 and 11 revealed two different TTDs, sharing little similarity in MTTs (120 and 169 days). As location 10 is nested in location 11, with both locations having a similar subcatchment area and percentage of riparian zone, we would have expected similar TTDs. Tributaries mostly showed shorter MTTs than the mainstream location where they discharge. Exceptions to this rule were location 3, 5, and 12 (Table 2).

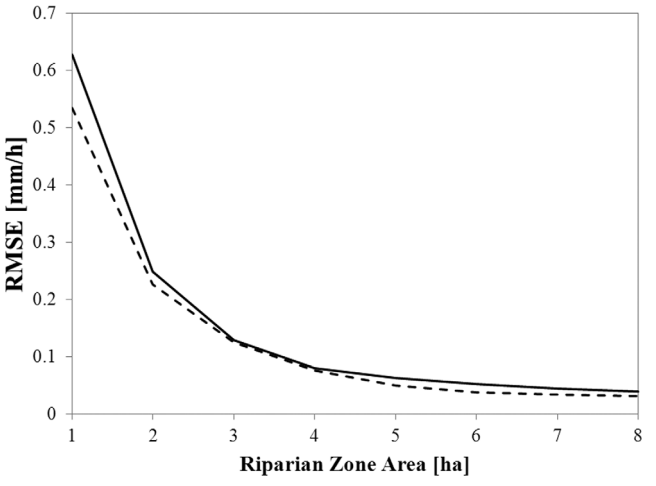

Figure 6. Relation between simulation performance (RMSE) of hydrograph simulations for Summer_09 (solid) and Summer_10 (dashed) and variable assumed sizes of the riparian zone area in the Wüstebach catchment (hydrologically active catchment during dry state).

As shown before, the RTD in the Wüstebach catchment was strongly affected by the riparian zone, because during the dry state only the riparian zone contributed to runoff. Therefore, we assumed that also the TTDs were highly influenced by the riparian zone. If the three optimized parameters of the TPLR model were not random combinations,

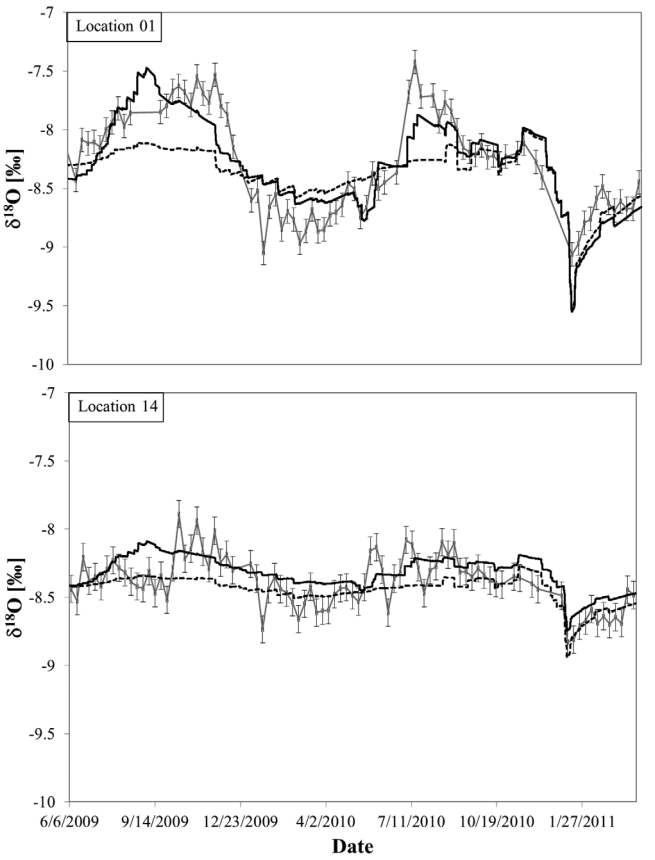

Figure 7. Stream isotope simulations for (top) location 1 and (bottom) 14. Observed isotope values (gray line with error bars), simulation result with changing active catchment area (black line) and simulation results with 38.5 ha active catchment area throughout the whole modeling period (dashed line). Location 1 with VE = 0.9788 and NSE = 0.74; location 14 with VE = 0.9855 and NSE = 0.34. Mark that strong deviations between observed and simulated values in summer 2009 are most likely caused by missing resolution of precipitation input.

the constantly well-saturated riparian zone should have been represented by the fast and the remaining part of the catchment by the slow reservoir of the TPLR model, as water conductance increases with increasing soil water content. The fast reservoir fraction (ϕ) should correspond to the proportion of the riparian zone within the subcatchment of each sampling location. A direct comparison revealed that the absolute differences were mostly less or equal to 10% (see Figure 9 and column "Diff" in Table 2). This indicated that the parameter sets were not physically meaningless and that the TTDs and their order can be explained by the influence of the riparian zone. The only exception was location 5, which showed an absolute difference of 16% for its relatively small subcatchment. Additionally, comparing the residence time of water in the fast and the slow reservoir, τ_f and τ_s, revealed that the model consistently chose very similar τ_f values, with larger variation in τ_s (Table 2). Although the model is conceptual, it appears that it was still able to find at least one explainable parameter.

Comparing the fraction of the riparian zone in each subcatchment to the respective MTT, we found higher proportions of riparian zone corresponding with shorter MTTs (Figure 10a). Main stream locations plotted relatively close together, with approximately the same percentage of riparian zone area. The exceptions to this are locations 1 and 2 near the spring of Wüstebach with a higher proportion of riparian zone. Locations 3, 12, 15, and 16 also group together, have low percentages of riparian zone, and the longest MTTs. Most tributary streams to the Wüstebach main stream (5, 8, 9, and 13) showed a variety of ranges of riparian zone fractions and MTTs. The linear regression between MTT and riparian zone area showed an R^2 of 0.50 with significance $p < 0.03$, indicating statistical significance. Comparing this to the TTDs in Figure 8a, it is apparent that locations with faster-reacting TTDs than the outlet usually have a higher percentage of riparian zone (with the outlet having 13%); conversely, slower-reacting TTDs have a smaller riparian zone fraction.

In contrast, no clear relationship between all subcatchment sizes and MTTs was found (Figure 10b). However, our data indicated a weak positive relationship between MTT and catchment size for the main stream locations. Additionally, tributaries and locations with long MTTs (possible groundwater influence, see section 5) seem to group together.

5. Discussion

Water balance results based on the whole modeling period and complete catchment area indicated an ET loss and storage change of 49%, which compares well with the Wüstebach catchment's 44% annual mean

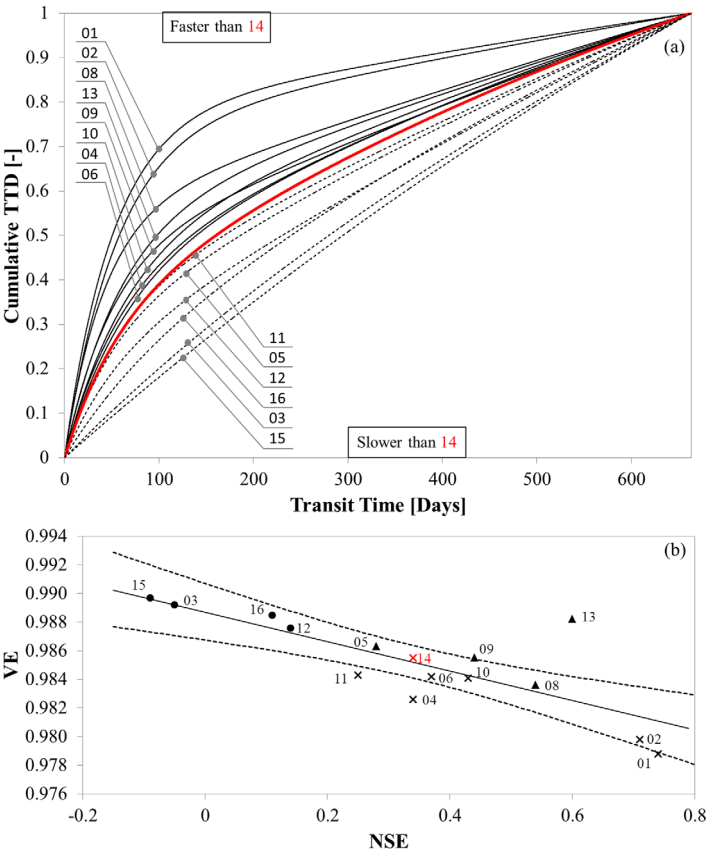

Figure 8. (a) Cumulative TTDs of all sampling locations (numerals), without subcatchment 7. The red line represents location 14 (outlet). Labels "Faster than 14" and "Slower than 14" indicate two subcatchment groups with shorter (upper group) and longer (lower group) MTTs compared to the outlet. (b) NSE and VE of all model simulations. Subcatchments have been divided in main stream (crosses) with the catchment's outlet highlighted (red cross), tributaries (triangles), and groundwater-dominated tributaries (circles). Regression line (solid line) with VE = −0.0103 * NSE + 0.989, R^2 of 0.63, significance $p < 0.0004$ and the 95% confidence intervals (dashed lines).

actual ET found by *Graf et al.* [2014]. The final p_{eff} sum used for TTD modeling indicated an ET loss of only 36%, explainable by the reduced active catchment area during the dry state, where less p_{eff} is lost in the well-saturated riparian zone.

Results of the cluster analysis showed that the split between dry and wet state occurred at a range between 35 and 37 vol % *SWCm*. Comparable seasonality in catchment behavior was also found in previous studies [*Birkel et al.*, 2012; *Heidbüchel et al.*, 2012]. Threshold-driven nonlinearities in a catchment's response, governed by soil moisture states, can be observed for many hydrological processes [*Zehe et al.*, 2007].

There are several possible physical explanations for the dry state's RTD lacking a slow component. We ruled out consistent infiltration-excess overland flow due to hydrophobicity and constant activation of preferential flow paths, as only one precipitation event (3 July 2010, 31 mm/h) showed clear signs of preferential flow in *Rosenbaum et al.* [2012]. Another explanation would be that the hydrological reaction of

Table 2. TTD Modeling Parameters and Subcatchment Characteristics[a]

Pos	VE (−)	NSE (−)	MTT (d)	τ_f (d)	τ_s (d)	ϕ (−)	Riparian (−)	Diff (−)	Area (ha)
1	0.9788	0.74	51	51	3226	0.37	0.32	0.05	3.9
2	0.9798	0.71	58	55	3209	0.33	0.35	0.02	4.6
3	0.9892	−0.05	280	278	5693	0.04	0.00	0.04	5.2
4	0.9826	0.34	134	56	1252	0.20	0.17	0.03	18.6
5	0.9863	0.28	186	49	1607	0.11	0.27	0.16	0.2
6	0.9842	0.37	140	63	1319	0.20	0.17	0.03	19.4
8	0.9836	0.54	72	41	4164	0.15	0.21	0.06	0.6
9	0.9855	0.44	111	48	3267	0.13	0.08	0.05	0.3
10	0.9841	0.43	120	63	2070	0.19	0.17	0.02	23.1
11	0.9843	0.25	169	54	1919	0.12	0.17	0.05	25.3
12	0.9876	0.14	231	54	2819	0.05	0.02	0.03	10.0
13	0.9882	0.60	98	58	4814	0.12	0.04	0.08	0.5
14	0.9855	0.34	160	57	1026	0.18	0.13	0.05	38.5
15	0.9897	−0.09	295	123	1472	0.00	0.02	0.02	6.3
16	0.9885	0.11	240	83	1472	0.07	0.06	0.01	11.4

[a]Pos, measurement location (Figure 1); VE, volumetric efficiency; NSE, Nash-Sutcliffe efficiency; MTT, mean transit time; τ_f, fast reservoir mean residence time for TTD h(τ); τ_s, slow reservoir mean residence time for TTD h(τ); ϕ, fast reservoir contribution for TTD h(τ); Riparian, percentage of riparian zone of total subcatchment area; Diff, absolute difference between fraction of riparian zone and ϕ; Area, total subcatchment area.

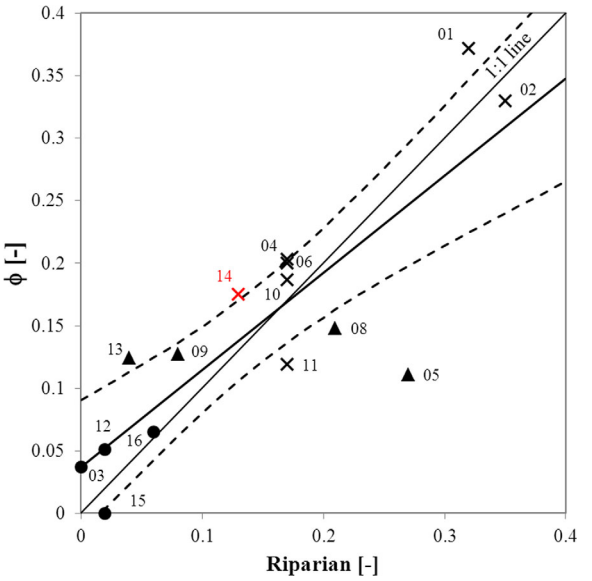

Figure 9. Fast reservoir contribution (ϕ) of the TPLR model for TTDs of all sampling locations (numerals) and the fraction of riparian soils of the respective subcatchments (Riparian), without subcatchment 7. Subcatchments have been divided in main stream (crosses) with the catchment's outlet highlighted (red cross), tributaries (triangles), and groundwater-dominated tributaries (circles). Thick line is regression line with $\phi = 0.777 *$ Riparian $+ 0.037$, with $R^2 = 0.71$, significance $p < 0.00008$ and the 95% confidence intervals (dashed lines).

the Wüstebach catchment is controlled by partial-area contributions [*Dunne and Black*, 1970]. According to *Dunne and Black* [1970], well-drained soils of the riparian zone were primarily responsible for fast infiltration-excess overland flow during summer storms in a small headwater catchment. At the same time, they observed that hillslopes did not produce significant subsurface flow during dry states and that precipitation was mainly stored in the soil. However, during wet states in winter, lateral hillslope subsurface flow (interflow) contributed to storm runoff generation. This concept of fast-reacting, well-saturated riparian zones and slow-reacting, unsaturated hillslopes has also been observed in other studies [*Rodgers et al*., 2005; *Tetzlaff et al*., 2009a]. We take this concept a step further by extending it from the event scale to the seasonal scale. In a similar way, *Beven and Freer* [2001] acknowledged the seasonality in the dynamics of the effective contributing area (a_{eff}) as an important control on the catchment response by including a variable a_{eff} in their dynamic TOPMODEL approach.

In our study, we argue that during the dry state the connectivity of hillslopes and the riparian zone is lost due to drying of the soil, while during the wet state it recovers. Thus, during winter months, with *SWCm* being typically larger than 35 vol %, both riparian zone and hillslopes are contributing to runoff, where the riparian zone contributes mainly the fast and the hillslopes mainly the slow-reacting parts of the winter RTD. During summer, the hillslope zones become hydrologically disconnected. Precipitation falling on the hillslopes is being stored in the soil, evaporated, and/or withdrawn by the spruce forest through transpiration. A hydrological disconnection of hillslopes from riparian zones has also been observed in *Jencso et al*. [2009] and *Detty and McGuire* [2010].

Bogena et al. [2013] used the one-dimensional soil hydraulic model HYDRUS 1-D [*Simunek et al*., 2008] to simulate spatially average soil moisture dynamics in the Wüstebach catchment neglecting lateral flow processes. They found that soil moisture dynamics could be successfully modeled using a no-flux lower boundary condition as long as the pressure head at the soil-bedrock interface is negative and using zero-pressure head as soon as the bottom of the profile becomes saturated. This procedure mimicked drainage by bedrock fissures acting as preferential pathways, laterally transporting water to the outlet. We complement this conceptual model of *Bogena et al*. [2013] for lateral flow processes using results of a field study of *Borchardt* [2012] to physically explain the hydrological disconnection of hillslopes. *Borchardt* [2012] found a distinct decrease in measured vertical hydraulic conductivities with soil depth and argued that this results in partial waterlogging at the top layer-base layer interface. The accumulated water preferentially flows laterally along this interface, with only minor percolation into the base layer. At locations where water gathers in depressions in the interface, percolation into the base layer is locally facilitated.

We postulate that during the dry state the lateral transport of soil water along this interface is negligible for the hillslope areas, as soil water is mainly consumed by forest transpiration. Additionally, no runoff is generated by the base layer of the hillslopes by lateral flow paths, as the bottom of the soil profile will be predominantly unsaturated. We argue the existence of a capillary barrier in the form of weathered bedrock, located at the transition zone between soil and solid bedrock. Under unsaturated conditions, this prevents

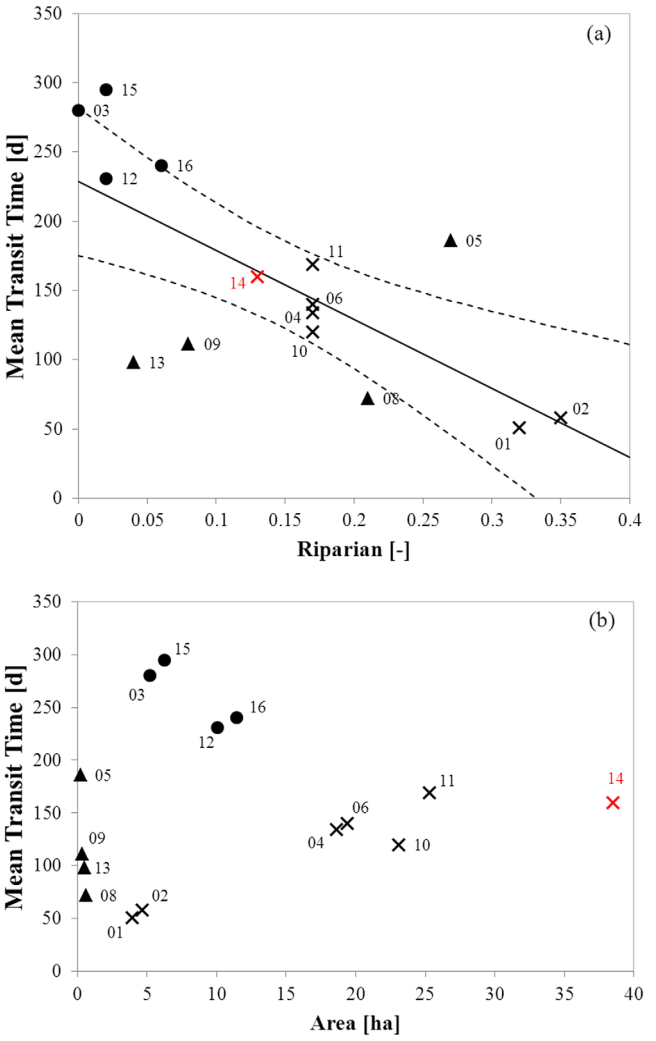

Figure 10. (a) Mean Transit Time (MTT) in days as a function of percentage of riparian zone area (Riparian) in each subcatchment (numerals) without subcatchment 7. Subcatchments have been divided in main stream (crosses) with the catchment's outlet highlighted (red cross), tributaries (triangles), and groundwater-dominated tributaries (circles). Solid line is a linear regression line for MTT = −497.82 * Riparian + 228.68 with $R^2 = 0.50$, significance $p < 0.03$ and the 95% confidence intervals (dashed lines). (b) MTT in days as a function of subcatchment area. Subcatchment locations are divided in different locations as described for Figure 10a.

vertical water movement to the bedrock fissures and lateral flow is also negligible. Thus, during dry states vertical flow paths dominate within the soil column, lateral water transport being negligible, and the hillslopes becoming hydrologically disconnected from the stream. This general dry condition can be different during extreme rainfall events, where lateral flow may occur. During the wet state the reduced ET demand, and thus higher soil water content, could result in the activation of lateral transport mechanisms, connecting the hillslopes to the stream: (1) lateral transport along the top layer-base layer interface through the soil matrix, accounting for slow transport, (2) saturation of the bottom of the soil profile and breakthrough of the capillary barrier, eventually with lateral water transport in the weathered bedrock layer, i.e., another slow transport mechanism, and (3) fast vertical water transport through the soil via macropores (I. Wiekenkamp, personal communication, 2014). The subsequent activation of bedrock fissures as lateral flow pathways, as modeled by *Bogena et al*. [2013], could account for the fast reaction of hillslope areas to precipitation in the wet state. They either react by transporting water to the stream delivering new water or by a pressure wave pushing out old water. Our conceptual model explains how soil water content could control the hydrological connectivity of hillslopes in the Wüstebach catchment. This dominance of vertical water transport during dry states and lateral water transport during wet states was also found in previous studies [e.g., *Grayson et al*., 1997]. With the available data we are, however, not able to analyze the lateral transport processes in the Wüstebach in more detail.

5.1. Can We Determine Subcatchment TTDs of Ungauged Stream Locations?

We found that stream isotope simulation markedly improved when applying the variable contributing catchment area approach. Additionally, we found that the stream isotope simulation performance increased when applying a correction of adding 0.5‰ to $\delta^{18}O$ C_{in} data, accounting for isotopic enrichment due to canopy interception processes. Previous studies found the increase in isotopic concentration to be inconsistent, showing a temporally nonstable, spatial pattern [*Allen et al*., 2013] or varying increases with rare decreases in isotope values [*Saxena*, 1986]. However, although the mean increase in $\delta^{18}O$ values for spruce stands of

about 0.3‰ in *Saxena* [1986] and 0.3‰ for Douglas fir in *Allen et al*. [2013] do not coincide with our added 0.5‰, it compares well to the mean increase for spruce of 0.56‰ of *Dewalle and Swistock* [1994].

Although we considered the seasonally changing active catchment area as well as the isotope signal changes due to throughfall, it was not possible to constrain all 15 TTD results. For example, locations 3, 11, 12, 15, and 16 showed comparatively low-NSE values, which might be the result of the strong influence of deep groundwater (see section 5.2), resulting in relatively stable isotope concentrations. *Stewart et al*. [2010] pointed out that stable isotopes cannot determine MTTs of greater than 4 years, as the variability in stream flow isotopes is lost with longer time frames. Generally, the model was able to constrain more dynamic isotope time series better than rather stable time series. An additional factor to consider is the low precipitation and stream water sampling frequency (weekly). *Birkel et al*. [2012] pointed out that weekly isotope observations will produce less certain TTDs estimates compared to shorter sampling intervals because information of temporal dynamics in the time series is lost. In our study, this happened due to averaging (precipitation) and due to time gaps (stream). Therefore, the already low isotope dynamics in the groundwater-influenced time series were further reduced due to the low sampling rate. The stream isotope simulation results generally showed less variability than the observed isotope time series (Figure 7). This can be explained by a missing dominant process in our model, accounting for, e.g., surface-runoff. However, we believe that the loss of temporal information due to the weekly sampling interval and the difference between average (precipitation) and grab (discharge) samples is the main reason for reduced variability in our simulation results.

The model parameter responsible for routing a certain percentage of precipitation through the fast reservoir (ϕ) showed good agreement with the percentage of riparian zone in each subcatchment, with the exception of location 5. We therefore assumed the TPLR's fast reservoir to be a good conceptualization of the riparian zone and that the slow reservoir represents the hillslopes. A possible explanation for the bigger deviation in location 5 is that the subsurface extent of its subcatchment could actually be larger than the topography-derived subcatchment area. The difference could also be explained by the fact that we used a single flow direction algorithm for catchment boundary delineation. This algorithm assumes that subsurface flow only occurs in the steepest downslope direction, while a multiple flow direction algorithm allows for subsurface flow in all downslope directions [*Jenson and Domingue*, 1988]. Nonetheless, the good agreement between ϕ and a measurable catchment characteristic indicates, if not necessarily quantitatively, but qualitatively correct results. Thus, we conclude that we were able to determine TTDs of ungauged stream locations to a mostly satisfying degree.

5.2. Spatial Variability of TTDs

Calculation of the 15 different TTDs yielded spatial information about the Wüstebach catchment, revealing possible sources of stream water. Overall, the outlet integrated the different TTDs observed in the Wüstebach catchment. Similar findings for the RTDs of nested catchments (ranging in size from 0.09 to 62.42 km^2) have been found in *McGuire et al*. [2005]. Locations that showed short MTTs and stronger dynamics in their seasonal stream isotope signal were most likely influenced by younger water. These locations usually had higher contributions of riparian zone in their respective subcatchments (e.g., locations 1, 2, and 8) as water can be routed fast through constantly saturated or near-saturated soil. Contrary to this, locations with longer MTTs (e.g., locations 3, 12, and 15) had less riparian zone contribution and less dynamics in their stream isotope signal. As location 3 receives its water from an old, artificial groundwater catchment system, we surmise that the sources of water of the other less dynamic time series locations are most likely groundwater too. The relationship between topographic indices and MTTs found in previous studies [e.g., *Tetzlaff et al*., 2009b] can be explained by the fact that topography is often a major influence on the distribution of saturated zones and thus the distribution of riparian zones and hillslopes [*Grabs et al*., 2009]. Comparing the TTDs of the main stream locations (1, 2, 4, 6, 10, 11, and 14) and tributaries we found that most main stream locations TTDs plotted quite close to each other (the exception being locations 1 and 2; see Figure 8a). The reason could be that the subcatchments of the main stream are nested, with major parts of downstream subcatchments consisting of upstream subcatchments, and thus not independent from each other. The tributary TTDs on the other hand are more divergent from each other, as their subcatchments are more distinct and separate. This can also be seen in the percentage of riparian zone of each tributary, where we found more variation than for main stream locations (Figure 10a).

5.3. Can We Explain the Spatial Variability of TTDs With Catchment Characteristics?

We found a negative correlation between the percentage of riparian zone and the MTT, as was already shown for mesoscale catchments [*Tetzlaff et al*., 2009a]. Similar to *McGuire et al*. [2005], we could not find a correlation between TTDs and the subcatchment size. What becomes apparent, however, is a relationship between subcatchment area and MTT for the main stream locations (Figure 10b). As already mentioned above, in the case of mainstream locations major parts of downstream subcatchments consist of upstream subcatchments, which could explain the observed relation between subcatchment size and MTT. Also, the tributaries and groundwater-influenced locations seemed to group together individually. However, it generally becomes apparent that at the small catchment scale it is also not the catchment size that has an influence on TTDs but flow path distributions governed by topography and soil cover, as has already been shown for mesoscale catchments before [*Asano and Uchida*, 2012; *Tetzlaff et al*., 2009a].

The shorter transit times in the riparian zone and the longer transit times in hillslope regions could be an explanation for the "old water phenomenon," where it was shown that most storm flow events mainly consist of old water, although the storm events deliver considerable runoff amounts [*Pearce et al*., 1986]. Fast transport mechanisms of storm water volumes are still under debate, for example immobile water increasing the water age of the mobile phase in *Duffy* [2010]. *Kirchner* [2003] summarized the old water phenomenon together with a chemical phenomenon by asking (a) how a catchment can store old water for a long time and then quickly release it during a storm and (b) how at the same time the chemistry of base flow and storm flow differ, although they both are mostly composed of old water. As it was suggested in other studies [e.g., *Inamdar and Mitchell*, 2007; *Jencso et al*., 2010; *McGlynn and Seibert*, 2003; *Ranalli and Macalady*, 2010] we also hypothesize that the riparian zone in the Wüstebach catchment is buffering water that stems from the hillslopes. We see from the TTDs that the transport through the soil matrix of the hillslopes is slow and leads to attenuated isotope signals. Therefore, the water has time to age before it reaches the saturated riparian zone via lateral flow pathways. During rainfall events, the resulting pressure wave (RTD) pushes the old water out of the riparian zone, creating the event hydrograph reaction. Thus, old water gets activated fast during an event as it does not need to travel far. A certain amount of event water will also discharge along more direct flow paths (overland flow, lateral preferential flow). This event water creates different chemical compositions in the stream. The remaining portion of event rainfall that follows slow flow paths (e.g., soil matrix) is at first new water that will eventually become old water over the course of its travel. When it eventually reaches the riparian zone, it will be stored and activated at the next event.

Alternative explanations of the "old water phenomenon" suggested in previous studies include activation of pre-event water as overland and subsurface storm flow [*Kienzler and Naef*, 2008] and rapidly rising groundwater reaching soil horizons of high lateral conductance [*Bishop et al*., 2004]. We ruled out both hypotheses in the case of the Wüstebach catchment, as there was no significant overland flow during the simulation period, while recently available, preliminary observations of groundwater levels do not indicate a rise to soil layers of significant lateral transport capabilities.

Indications of the riparian zone's soil water being old water from the hillslopes were found in a comparison of the main stream isotope time series of the individual stream locations (not shown). In the scenario of the riparian zone's water actually being relatively young water, every main stream location should show higher amplitudes in their isotope signal during the dry state, taking into account that only the fast-reacting riparian zone remains hydrologically connected. However, we observed diminishing amplitudes in the stream isotope signals downstream from the spring, with locations 1 and 2 showing high amplitudes and subsequent locations lower ones. This indicates the existence of old water in the riparian zone. The riparian zone fraction to the respective catchment area decreases downstream from 32% (location 1, spring) to 13% (location 14, outlet), and consequently the potential contributions of old water from hillslopes to the riparian zone via slow pathways originating from wet states increases. This explains the decrease in the amplitudes of the isotope tracer signals during the dry states observed at downstream locations, as each downstream location's riparian zone collects water from a larger fraction of hillslope. This also implies that the isotopic composition of the riparian zone is not spatially uniform, but that there is a gradient downstream towards more groundwater-like isotopic signatures.

5.4. Limitations

A limitation of our proposed method is the assumption that p_{eff} is spatially homogeneous for a small-scale catchment. Small catchments with different land use types, e.g., forest and bare soil, would have spatially

heterogeneous evapotranspiration characteristics and thus not a uniform p_{eff}. We assume that a small number of deviations in the p_{eff} time series, e.g., due to localized storm cells, will have minimal effect on a weekly stream isotope time series where simulation results tend to focus on long-term trends. In our study there was only one event in 2 years which we assumed to be a localized convective storm cell. However, in case of systematic deviations we expect a nonnegligible error in TTDs estimates. The catchment also needs to be sufficiently small to justify this assumption. We suggest a range of maximum catchment sizes between 1 and 5 km^2, keeping in mind that this may depend on climate and other factors, e.g., the extent of uniform vegetation cover.

Judging by the good NSE values, we saw that the p_{eff} time series derived from the outlet seemed to work for location 1, which is one of the furthest locations from the outlet (Figure 1). Thus, it seems that for the small and comparably homogeneous Wüstebach catchment the assumption of p_{eff} is valid.

6. Conclusions

We have presented a method to calculate TTDs for gauged and ungauged stream locations using the conceptual model TRANSEP, given that p_{eff} is spatially uniform. The modeling of the isotope time series was only possible with information gained by the dense measurement network available at this study site. We found a critical mean soil water content of 35 vol % where the catchment switches between two different hydrological behaviors. This closely resembles the partial-area contribution concept by *Dunne and Black* [1970], who observed such a behavior for single storm events. TTDs modeling results were generally solid, with exceptions though, and supported by comparing the model parameter of fast reservoir contribution to the measurable proportion of the riparian zone in each subcatchment. Results suggested that fast flow paths are more often activated in the riparian zone compared to hillslopes, as the riparian zone is more often well saturated. RTDs indicated that hillslopes become hydrologically disconnected during dry states. We found that even in small catchments like the Wüstebach (38.5 ha) the MTTs were closely linked to the surface area of riparian zone and not to the size of its subcatchments. The different hydrological behavior of riparian and hillslope areas may prove to be instrumental in explaining the amount of old water that gets activated during storm events, which is often observable in tracer studies.

Acknowledgments
We gratefully acknowledge the support by the SFB-TR32 "Pattern in Soil-Vegetation-Atmosphere Systems: Monitoring, Modelling, and Data Assimilation" funded by the Deutsche Forschungsgemeinschaft (DFG) and TERENO (Terrestrial Environmental Observatories) funded by the Helmholtz-Gemeinschaft. Holger Wissel, Willi Benders, Leander Fürst, and Ferdinand Engels are thanked for supporting the isotope analysis and ongoing maintenance of the experimental setup, and Heinz Vos for advice on cluster analysis. We especially acknowledge the contribution of two anonymous reviewers and Henry Lin for valuable advice.

References

Abbaspour, K. C., R. Schulin, and M. T. van Genuchten (2001), Estimating unsaturated soil hydraulic parameters using ant colony optimization, *Adv. Water Resour.*, *24*(8), 827–841.
Allen, S. T., J. R. Brooks, R. F. Keim, B. J. Bond, and J. J. McDonnell (2013), The role of pre-event canopy storage in throughfall and stemflow by using isotopic tracers, *Ecohydrology*, *7*, 858–868, doi:10.1002/eco.1408.
Asano, Y., and T. Uchida (2012), Flow path depth is the main controller of mean base flow transit times in a mountainous catchment, *Water Resour. Res.*, *48*, W03512, doi:10.1029/2011WR010906.
Beven, K., and J. Freer (2001), A dynamic TOPMODEL, *Hydrol. Processes*, *15*(10), 1993–2011.
Birkel, C., C. Soulsby, D. Tetzlaff, S. Dunn, and L. Spezia (2012), High-frequency storm event isotope sampling reveals time-variant transit time distributions and influence of diurnal cycles, *Hydrol. Processes*, *26*(2), 308–316.
Bishop, K., J. Seibert, S. Koher, and H. Laudon (2004), Resolving the Double Paradox of rapidly mobilized old water with highly variable responses in runoff chemistry, *Hydrol. Processes*, *18*(1), 185–189.
Bogena, H. R., M. Herbst, J. A. Huisman, U. Rosenbaum, A. Weuthen, and H. Vereecken (2010), Potential of wireless sensor networks for measuring soil water content variability, *Vadose Zone J.*, *9*(4), 1002–1013.
Bogena, H. R., J. A. Huisman, R. Baatz, H.-J. Hendriks-Franssen, and H. Vereecken (2013), Accuracy of the cosmic-ray soil water content probe in humid forest ecosystems: The worst case scenario, *Water Resour. Res.*, *49*, 5778–5791, doi:10.1002/wrcr.20463.
Borchardt, H. (2012), Einfluss periglazialer Deckschichten auf Abflusssteuerung am Beispiel des anthropogen überprägten Wüstebaches (Nationalpark Eifel), PhD diss., Lehrstuhl für Physische Geogr. und Geoökologie, Fak. für Georessourcen und Materialtechnik, Rheinisch-Westfälische Tech. Hochsch. Aachen, Aaachen, Germany.
Cornelissen, T., B. Diekkrüger, and H. R. Bogena (2014), Significance of scale and lower boundary condition in the 3D simulation of hydrological processes and soil moisture variability in a forested headwater catchment, *J. Hydrol.*, doi:10.1016/j.jhydrol.2014.01.060, in press.
Craig, H. (1961), Isotopic variations in meteoric waters, *Science*, *133*(346), 1702–1703.
Criss, R. E., and W. E. Winston (2008), Do Nash values have value? Discussion and alternate proposals, *Hydrol. Processes*, *22*(14), 2723–2725.
Detty, J. M., and K. J. McGuire (2010), Topographic controls on shallow groundwater dynamics: Implications of hydrologic connectivity between hillslopes and riparian zones in a till mantled catchment, *Hydrol. Processes*, *24*(16), 2222–2236.
Dewalle, D. R., and B. R. Swistock (1994), Differences in O-18 content of throughfall and rainfall in hardwood and coniferous forests, *Hydrol. Processes*, *8*(1), 75–82.
Duffy, C. J. (2010), Dynamical modelling of concentration-age-discharge in watersheds, *Hydrol. Processes*, *24*(12), 1711–1718.
Dunne, T., and R. D. Black (1970), Partial area contributions to storm runoff in a small New England Watershed, *Water Resour. Res.*, *6*(5), 1296–1366.
Etmann, M. (2009), Dendrologische Aufnahmen im Wassereinzugsgebiet Oberer Wüstebach anhand verschiedener Mess- und Schätzverfahren, MS thesis, Institut für Landschaftsökologie, Univ. of Münster, Münster, Germany.

Fraley, C., and A. E. Raftery (2002), Model-based clustering, discriminant analysis, and density estimation, *J. Am. Stat. Assoc.*, *97*(458), 611–631.
Gonfiantini, R. (1978), Standards for stable isotope measurements in natural compounds, *Nature*, *271*(5645), 534–536.
Grabs, T., J. Seibert, K. Bishop, and H. Laudon (2009), Modeling spatial patterns of saturated areas: A comparison of the topographic wetness index and a dynamic distributed model, *J. Hydrol.*, *373*(1–2), 15–23.
Graf, A., H. R. Bogena, C. Drüe, H. Hardelauf, T. Pütz, G. Heinemann, and H. Vereecken (2014), Spatiotemporal relations between water budget components and soil water content in a forested tributary catchment, *Water Resour. Res.*, *50*, doi:10.1002/2013WR014516.
Grayson, R. B., A. W. Western, F. H. S. Chiew, and G. Bloschl (1997), Preferred states in spatial soil moisture patterns: Local and nonlocal controls, *Water Resour. Res.*, *33*(12), 2897–2908.
Heidbüchel, I., P. A. Troch, S. W. Lyon, and M. Weiler (2012), The master transit time distribution of variable flow systems, *Water Resour. Res.*, *48*, W06520, doi:10.1029/2011WR011293.
Herrmann, A., S. Bahls, W. Stichler, F. Gallart, and J. Latron (1999), Isotope hydrological study of mean transit times and related hydrogeological conditions in Pyrenean experimental basins (Vallcebre, Catalonia), in *Integrated Methods in Catchment Hydrology—Tracer, Remote Sensing and New Hydrometric Techniques*, *IAHS Publ. 258*, pp. 101–109.
Hrachowitz, M., C. Soulsby, D. Tetzlaff, J. J. C. Dawson, and I. A. Malcolm (2009a), Regionalization of transit time estimates in montane catchments by integrating landscape controls, *Water Resour. Res.*, *45*, W05421, doi:10.1029/2008WR007496.
Hrachowitz, M., C. Soulsby, D. Tetzlaff, J. J. C. Dawson, S. M. Dunn, and I. A. Malcolm (2009b), Using long-term data sets to understand transit times in contrasting headwater catchments, *J. Hydrol.*, *367*(3–4), 237–248.
Inamdar, S. P., and M. J. Mitchell (2007), Contributions of riparian and hillslope waters to storm runoff across multiple catchments and storm events in a glaciated forested watershed, *J. Hydrol.*, *341*(1–2), 116–130.
Jakeman, A. J., and G. M. Hornberger (1993), How much complexity is warranted in a rainfall-runoff model, *Water Resour. Res.*, *29*(8), 2637–2649.
Jencso, K. G., B. L. McGlynn, M. N. Gooseff, S. M. Wondzell, K. E. Bencala, and L. A. Marshall (2009), Hydrologic connectivity between landscapes and streams: Transferring reach-and plot-scale understanding to the catchment scale, *Water Resour. Res.*, *45*, W04428, doi:10.1029/2008WR007225.
Jencso, K. G., B. L. McGlynn, M. N. Gooseff, K. E. Bencala, and S. M. Wondzell (2010), Hillslope hydrologic connectivity controls riparian groundwater turnover: Implications of catchment structure for riparian buffering and stream water sources, *Water Resour. Res.*, *46*, W10524, doi:10.1029/2009WR008818.
Jenson, S. K., and J. O. Domingue (1988), Extracting topographic structure from digital elevation data for geographic information-system analysis, *Photogramm. Eng. Remote Sens.*, *54*(11), 1593–1600.
Kienzler, P. M., and F. Naef (2008), Subsurface storm flow formation at different hillslopes and implications for the "old water paradox," *Hydrol. Processes*, *22*(1), 104–116.
Kirchner, J. W. (2003), A double paradox in catchment hydrology and geochemistry, *Hydrol. Processes*, *17*(4), 871–874.
Maloszewski, P., W. Rauert, P. Trimborn, A. Herrmann, and R. Rau (1992), Isotope hydrological study of mean transit times in an Alpine Basin (Wimbachtal, Germany), *J. Hydrol.*, *140*(1–4), 343–360.
McDonnell, J. J., et al. (2010), How old is streamwater? Open questions in catchment transit time conceptualization, modelling and analysis, *Hydrol. Processes*, *24*, 1745–1754, doi:10.1002/hyp.7796.
McGlynn, B. L., and J. Seibert (2003), Distributed assessment of contributing area and riparian buffering along stream networks, *Water Resour. Res.*, *39*(4), 1082, doi:10.1029/2002WR001521.
McGuire, K. J., and J. J. McDonnell (2006), A review and evaluation of catchment transit time modeling, *J. Hydrol.*, *330*(3–4), 543–563.
McGuire, K. J., J. J. McDonnell, M. Weiler, C. Kendall, B. L. McGlynn, J. M. Welker, and J. Seibert (2005), The role of topography on catchment-scale water residence time, *Water Resour. Res.*, *41*, W05002, doi:10.1029/2004WR003657.
Nash, J. E., and J. V. Sutcliffe (1970), River flow forecasting through conceptual models: Part I—A discussion of principles, *J. Hydrol.*, *10*(3), 282–290.
Pearce, A. J., M. K. Stewart, and M. G. Sklash (1986), Storm runoff generation in humid headwater catchments. 1. Where does the water come from?, *Water Resour. Res.*, *22*(8), 1263–1272.
Ranalli, A. J., and D. L. Macalady (2010), The importance of the riparian zone and in-stream processes in nitrate attenuation in undisturbed and agricultural watersheds—A review of the scientific literature, *J. Hydrol.*, *389*(3–4), 406–415.
Richter, D. (1995), Ergebnisse methodischer Untersuchungen zur Korrektur des systematischen Meßfehlers des Hellmann-Niederschlagsmessers, 93 S. pp., Selbstverl. des Dt. Wetterdienstes, Offenbach am Main.
Richter, F. (2008), Bodenkarte zur Standorterkundung. Verfahren Quellgebiet Wüstebachtal (Forst), Geologischer Dienst Nordrhein-Westfalen, Krefeld, Germany.
Rinaldo, A., K. J. Beven, E. Bertuzzo, L. Nicotina, J. Davies, A. Fiori, D. Russo, and G. Botter (2011), Catchment travel time distributions and water flow in soils, *Water Resour. Res.*, *47*, W07537, doi:10.1029/2011WR010478.
Roa-Garcia, M. C., and M. Weiler (2010), Integrated response and transit time distributions of watersheds by combining hydrograph separation and long-term transit time modeling, *Hydrol. Earth Syst. Sci.*, *14*(8), 1537–1549.
Rodgers, P., C. Soulsby, S. Waldron, and D. Tetzlaff (2005), Using stable isotope tracers to assess hydrological flow paths, residence times and landscape influences in a nested mesoscale catchment, *Hydrol. Earth Syst. Sci.*, *9*(3), 139–155.
Rosenbaum, U., H. R. Bogena, M. Herbst, J. A. Huisman, T. J. Peterson, A. Weuthen, A. W. Western, and H. Vereecken (2012), Seasonal and event dynamics of spatial soil moisture patterns at the small catchment scale, *Water Resour. Res.*, *48*, W10544, doi:10.1029/2011WR011518.
Saxena, R. K. (1986), Estimation of canopy reservoir capacity and o-18 fractionation in throughfall in a pine forest, *Nord. Hydrol.*, *17*(4–5), 251–260.
Shaman, J., M. Stieglitz, and D. Burns (2004), Are big basins just the sum of small catchments?, *Hydrol. Processes*, *18*(16), 3195–3206.
Simunek, J., M. T. van Genuchten, and M. Sejna (2008), Development and applications of the HYDRUS and STANMOD software packages and related codes, *Vadose Zone J.*, *7*(2), 587–600, doi:10.2136/vzj2007.0077.
Soulsby, C., D. Tetzlaff, and M. Hrachowitz (2009), Tracers and transit times: Windows for viewing catchment scale storage?, *Hydrol. Processes*, *23*(24), 3503–3507.
Stewart, M. K., and B. D. Fahey (2010), Runoff generating processes in adjacent tussock grassland and pine plantation catchments as indicated by mean transit time estimation using tritium, *Hydrol. Earth Syst. Sci.*, *14*(6), 1021–1032.
Stewart, M. K., U. Morgenstern, and J. J. McDonnell (2010), Truncation of stream residence time: How the use of stable isotopes has skewed our concept of streamwater age and origin, *Hydrol. Processes*, *24*, 1646–1659, doi:10.1002/hyp.7576.

Tetzlaff, D., J. J. McDonnell, S. Uhlenbrook, K. J. McGuire, P. W. Bogaart, F. Naef, A. J. Baird, S. M. Dunn, and C. Soulsby (2008), Conceptualizing catchment processes: Simply too complex?, *Hydrol. Processes*, *22*(11), 1727–1730.

Tetzlaff, D., J. Seibert, and C. Soulsby (2009a), Inter-catchment comparison to assess the influence of topography and soils on catchment transit times in a geomorphic province; the Cairngorm mountains, Scotland, *Hydrol. Processes*, *23*(13), 1874–1886.

Tetzlaff, D., J. Seibert, K. J. McGuire, H. Laudon, D. A. Burn, S. M. Dunn, and C. Soulsby (2009b), How does landscape structure influence catchment transit time across different geomorphic provinces?, *Hydrol. Processes*, *23*(6), 945–953.

Weiler, M., B. L. McGlynn, K. J. McGuire, and J. J. McDonnell (2003), How does rainfall become runoff? A combined tracer and runoff transfer function approach, *Water Resour. Res.*, *39*(11), 1315, doi:10.1029/2003WR002331.

Williams, A. G., J. F. Dowd, and E. W. Meyles (2002), A new interpretation of kinematic stormflow generation, *Hydrol. Processes*, *16*(14), 2791–2803.

Zacharias, S., et al. (2011), A network of terrestrial environmental observatories in Germany, *Vadose Zone J.*, *10*(3), 955–973.

Zehe, E., H. Elsenbeer, F. Lindenmaier, K. Schulz, and G. Bloschl (2007), Patterns of predictability in hydrological threshold systems, *Water Resour. Res.*, *43*, W07434, doi:10.1029/2006WR005589.